Orography in a Contour Dynamics Model of Large-Scale Atmospheric Flow

M. H. P. AMBAUM AND W. T. M. VERKLEY

Royal Netherlands Meteorological Institute, De Bilt, the Netherlands

(Manuscript received 25 August 1994, in final form 12 January 1995)

ABSTRACT

The influence of orography on the structure of stationary planetary Rossby waves is studied in the context of a contour dynamics model of the large-scale atmospheric flow. Orography of infinitesimal and finite amplitude is studied using analytical and numerical techniques. Three different types of orography are considered: idealized orography in the form of a global wave, idealized orography in the form of a local table mountain, and the earth's orography. The study confirms the importance of resonances, both in the infinitesimal orography and in the finite orography cases. With finite orography the stationary waves organize themselves into a one-dimensional set of solutions, which due to the resonances, is piecewise connected. It is pointed out that these stationary waves could be relevant for atmospheric regimes.

1. Introduction

Maps of potential vorticity on isentropic surfaces (isentropic potential vorticity maps) show that the potential vorticity in the stratosphere is generally much larger than in the troposphere. Moreover, isentropic potential vorticity in both the troposphere and the stratosphere is relatively uniform, with the gradients concentrated in a narrow band at the tropopause. Being the transition between high and low potential vorticity values, the tropopause is therefore a major factor in determining the structure of the atmospheric potential vorticity field. In light of the invertibility principle (Hoskins et al. 1985), which states that for balanced flow the potential vorticity structure determines the structure of all other meteorological fields (assuming knowledge of the potential temperature at the ground), the tropopause is to play a key role in the dynamics of large-scale atmospheric flow.

In Verkley (1994, hereafter referred to as VE) this fact was used as the basis of a concise model of the atmospheric circulation. In this model the dynamics was assumed to be confined to a single level of constant potential temperature, which level was assumed to cut through the tropopause. The potential vorticity on this level was then taken to be piecewise uniform, with constant high values representing stratospheric air, constant low values representing tropospheric air, and the discontinuity representing the tropopause. This was shown to lead to a contour dynamics system, that is, a system completely formulated in terms of the discontinuity, by assuming that the dynamics of potential vorticity on an isentropic surface is governed by the equivalent barotropic vorticity equation.[1] In the present paper we wish to extend this contour dynamics model by incorporating orography. This is accomplished by adding an orographic term to the equivalent barotropic vorticity and requiring the latter to be piecewise uniform.

The present study fits in a long tradition of research concerning the influence of orography on the large-scale atmospheric flow. An early summary of theoretical studies is given in Queney (1948) and two subsequent highlights are Charney and Eliassen (1949) and Bolin (1950). In the latter study it was argued that the orography is more important in determining the structure of the stationary planetary waves than spatial differences in diabatic heating. Many other studies have followed since, using models of different degrees of sophistication—ranging from relatively simple analytical models like Bolin's to complex general circulation models of the atmosphere. A review of research until 1965 is given by Saltzman (1968). Examples of quite recent analytical studies are Charney and DeVore (1979) and Pedlosky (1981), who showed that the presence of orography in combination with resonance leads to multiple stationary states. These multiple flow equilibria usually contain a state that is rather zonal and another that has a pronounced wavelike character. For this reason these states are considered as an explanation for the existence of atmospheric regimes like blocking.

Corresponding author address: M. H. P. Ambaum, Royal Netherlands Meteorological Institute, P.O. Box 201, 3730 AE De Bilt, the Netherlands.

[1] In the general literature on two-dimensional fluid mechanics the equivalent barotropic vorticity is often called the quasigeostrophic potential vorticity.

The technique of contour dynamics was originally devised by Zabusky et al. (1979). Since then it has found numerous applications in the study of two-dimensional flows (for a review see Pullin 1992), especially in the context of vortex equilibria. In the latter field the technique provided us, by computational methods, with new equilibria besides the already known circular and elliptical vorticity distributions. These new equilibria comprise, for example, m-fold symmetric single-vortex states and translating two-vortex states (Deem and Zabusky 1978), corotating two-vortex states (Saffman and Szeto 1980) and corotating multiple-vortex states (Dritschel 1985). Polvani and Dritschel (1993) extend the family of m-fold symmetric single-vortex states and corotating multiple-vortex states to the geometry of a sphere in a barotropic model. The technique they use for finding equilibria consists of an iteration process, where in every iteration step the contour is modified, such that in a linear approximation the contour becomes stationary. Using another iteration process, Verkley (1994) finds m-fold symmetric single-vortex equilibria on a sphere in an equivalent barotropic model. He was not able to find multiple-vortex equilibria.

The application of contour dynamics techniques to the atmosphere is relatively new and is mainly concentrated on time-dependent studies of the stratospheric polar vortex in order to understand wave breaking phenomena like observed by McIntyre and Palmer (1983). The studies often contain a simple orographic term, much the same way as we include it, in order to induce waves on the polar vortex. Some examples are Polvani and Plumb (1992), Waugh (1993), Waugh et al. (1994), and Nakamura and Plumb (1994). In the present study we introduce different types of orography, including the earth's orography. We concentrate on stationary solutions of the model. Thus, we find (to our knowledge for the first time) *asymmetric* single-vortex states. It is showed that the basic facts concerning the influence of orography—including the existence of multiple stationary states—are reproduced in this contour dynamics model of the atmosphere.

The contour dynamics model and the inclusion of orography therein, are outlined in section 2. Three different types of orography are studied: idealized global orography in the form of a single wave, an idealized local table mountain, and the earth's orography. First we review the case of no orography in section 3 together with linear and nonlinear free Rossby waves, that is, the m-fold symmetric single-vortex states, in terms of their energy and enclosed area. Then we study the influence of infinitesimal orography in section 4. This is done by linearizing around a zonal contour and then calculating analytically the linear perturbation that makes the perturbed contour stationary in the presence of vanishingly small orography. The expressions we obtain have a well-known structure (see Egger 1978) and show the importance of resonances, that is, the existence of free stationary Rossby waves, in determining the dominant structure of the resulting response. By changing the latitude of the basic zonal contours one passes through these resonances and there the dominant response changes sign, becoming infinite at the resonances themselves. In section 5 we use a numerical technique to construct stationary contours in the presence of finite-amplitude orography. Part of the technique consists of constructing families of stationary contours in the presence of increasing mountain height. We will see that this procedure effectively maps every zonal contour—which is stationary without orography—onto a contour that is stationary with orography. Close to zonal contours that are resonant the map depends sensitively on the direction from which the resonance is approached, generally resulting in a solution diagram in which there are several branches. In the case of realistic orography these branches are argued to be interesting from the perspective of atmospheric regimes. A summary and an outlook are given in section 6.

2. Orography and contour dynamics

The starting point of our investigations is the equivalent barotropic vorticity equation on a spherical earth with radius $a = 6.371 \times 10^6$ m rotating with angular velocity $\Omega = 7.292 \times 10^{-5}\ \mathrm{s}^{-1}$. Lengths are expressed in units of a and time in units of Ω^{-1}. The equations read

$$\frac{\partial q}{\partial t} + \mathbf{v}\cdot\nabla q = 0, \tag{1a}$$

$$q = f + \zeta - F\psi + \tau. \tag{1b}$$

The first equation expresses material conservation of potential vorticity q. The velocity field $\mathbf{v}$ has components u and v along the unit vectors $\mathbf{i}$ and $\mathbf{j}$, which point in the direction of increasing longitude λ and latitude ϕ and form a right-handed set of unit vectors together with $\mathbf{k}$, which points vertically upward. The nondivergent velocity field is given in terms of the streamfunction ψ by $\mathbf{v} = \mathbf{k} \times \nabla\psi$. Equation (1b) is the quasigeostrophic approximation of Ertel's potential vorticity. The first contribution to q is the planetary vorticity. In units of Ω it equals

$$f = 2\sin\phi. \tag{2}$$

The second contribution is the relative vorticity ζ, that is, the vertical component of the curl of $\mathbf{v}$, which is given in terms of the streamfunction ψ by $\zeta = \nabla^2\psi$. The third contribution to the potential vorticity is the stretching term $-F\psi$ and is the quasigeostrophic representation of the vortex stretching effect due to the stratification. The Froude number F in this term is defined as $F = L_R^{-2}$, where L_R is the Rossby radius in units of a. We will take $L_R = 1/10$, which amounts to a Rossby radius of 637.1 km. This choice is motivated

in VE. It will lead to realistic velocities at the jet and on the rest of the sphere. In the same way, vortex stretching by orography is represented by the last term in the expression for q,

$$\tau = f\eta, \tag{3}$$

where η is given by $\eta = h/H$, with h the height of the orography and H an appropriate scale height, which we set to 10 km. From now on we will refer to the quantity τ simply as "the orography." This extra term in the potential vorticity is often referred to as "topographic forcing," (cf. Waugh 1993). We like to stress though that the term does not inject energy in the flow. Its role is equivalent to that of the Coriolis parameter.

It will be convenient to assume that τ can be written as a finite series of spherical harmonics Y_{mn}. This is not an essential feature, but it will simplify the calculations on some occasions. So τ will be written as

$$\tau = \tau_{00} + \sum_{n=1}^{N} \sum_{m=-n}^{n} \tau_{mn} Y_{mn}, \tag{4}$$

where $Y_{mn}(\lambda, \phi) = P_n^m(\sin\phi)e^{im\lambda}$ with $P_n^m(x)$ the associated Legendre polynomials of order m and degree n. The spherical harmonics Y_{mn} are eigenfunctions of the Laplace operator ∇^2 on the sphere with eigenvalue $-n(n+1)$ and are normalized such that

$$\frac{1}{4\pi}\int_S Y^*_{mn} Y_{m'n'}\, dS = \delta_{mm'}\delta_{nn'}, \tag{5}$$

where the superscript * denotes complex conjugation. Defining $P_n^{-m}(\sin\phi) = P_n^m(\sin\phi)$, we must have $\tau_{-mn} = \tau^*_{mn}$ as τ is a real-valued field.

We now assume that the q field is piecewise uniform. We will thus assume that q has the constant value q_1 in a region R_1 (around the north pole) and another constant value q_0 on the rest of the sphere, denoted by R_0. The boundary between R_1 and R_0 is assumed to be a single closed curve B, see Fig. 1. So the potential vorticity q is assumed to be of the form

$$q(\mathbf{r}) = q_0 + q_B(\mathbf{r}), \tag{6}$$

with

$$q_B(\mathbf{r}) = \begin{cases} q_1 - q_0, & \mathbf{r} \in R_1 \\ 0, & \mathbf{r} \in R_0. \end{cases} \tag{7}$$

Due to q being materially conserved, this idealized distribution of potential vorticity will remain intact in the course of time. So at all times the position of the contour B uniquely determines the structure of the potential vorticity field. In order to calculate how the position of the contour changes as time proceeds we need to know the velocity field at the position of the contour. We start by calculating the streamfunction ψ from the equation

$$\nabla^2\psi - F\psi = q - f - \tau = q_0 - f - \tau + q_B. \tag{8}$$

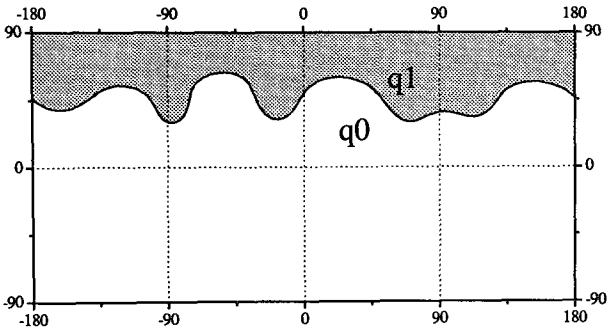

FIG. 1. Potential vorticity field as used in our contour dynamics model. The shaded region is the region R_1 with high potential vorticity value q_1. The unshaded region R_0 has the lower potential vorticity value q_0. Their common boundary B is the contour that determines the complete potential vorticity field and all quantities derived from it.

This is a nonhomogeneous linear equation in ψ. The solution of this equation can be written as

$$\psi = \psi_0 + \psi_f + \psi_\tau + \psi_B, \tag{9}$$

where ψ_0, ψ_f, ψ_τ, and ψ_B respectively refer to the four source terms on the right-hand side of (8). As the first three source terms can be written in terms of spherical harmonics (note that q_0 is proportional to Y_{00} and f is proportional to Y_{01}), their contributions to the solution of (8) are straightforward. We have

$$\psi_0(\mathbf{r}) = -\frac{q_0}{F} \tag{10}$$

$$\psi_f(\mathbf{r}) = \frac{f(\mathbf{r})}{F+2} \tag{11}$$

$$\psi_\tau(\mathbf{r}) = \frac{\tau_{00}}{F} + \sum_{n=1}^{N} \sum_{m=-n}^{n} \frac{\tau_{mn}}{F + n(n+1)} Y_{mn}(\mathbf{r}). \tag{12}$$

These three contributions to the streamfunction are independent of the contour's position, the latter contribution being determined by the orography. We will take $q_0 = 0$, which results in $\psi_0 = 0$. We have this freedom of choice because of the stretching term in the definition of q. One can easily add up a constant to the streamfunction without changing the dynamics, but, according to (10), adding a constant to the streamfunction is equivalent to adding a constant to the potential vorticity. In the barotropic case this freedom is lost because the global average of the left-hand side of (8) vanishes when $F = 0$.

In Fig. 2 we present three types of orography with their corresponding $\psi_f + \psi_\tau$, which will be used throughout this paper to illustrate the theory. These are a single Y_{33} wave, a table mountain, and the earth's mountains. The Y_{33} orography is a linear combination of the single wave $P_3^3(\sin\phi)\cos 3\lambda$ and a constant, such as to make the height vary between 0 km and 4.2 km. The table mountain is a flat round mountain with its

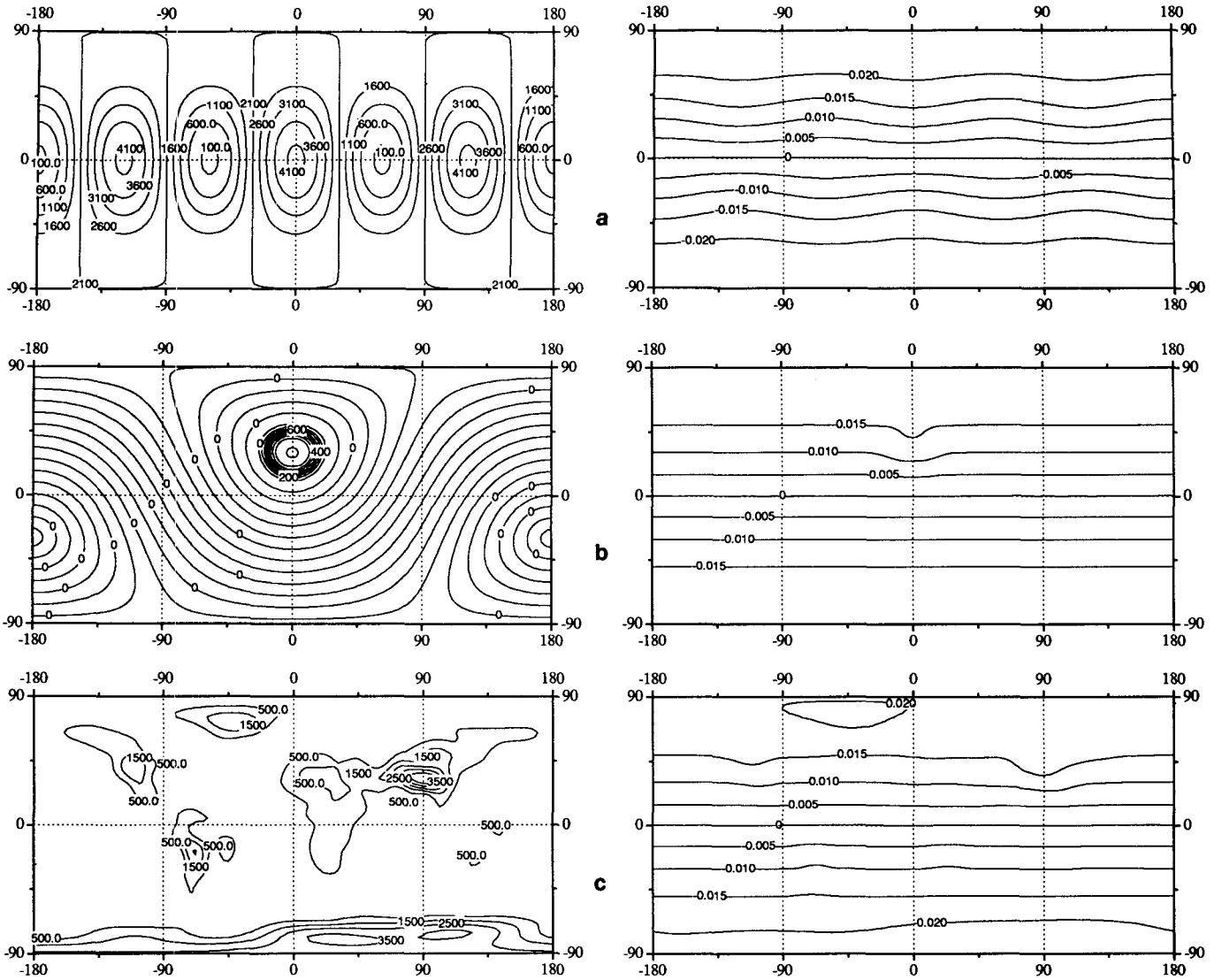

FIG. 2. The three types of orography (left panels) and their corresponding $\psi_f + \psi_\tau$ (right panels). (a) Orography, which is a linear combination of the Y_{00} and the Y_{33} spherical harmonics. The height varies from 0 km at the lowest points to 4.2 km at the highest points. (b) $T21$ spectral representation of a circular table mountain at 30° latitude, 0° longitude with radius 15°. The height is 1.4 km. Due to the finite truncation the height actually varies between −121 m and 1526 m. (c) $T21$ spectral representation of the earth's orography. The height varies from −606 m to 5488 m.

center at 30° lat, 0° long with a radius of 15° and a height of 1.4 km. Finally, we also used the earth's orography. In the model the table mountain and the earth's mountains are represented spectrally with a T21 triangular truncation (i.e., the spherical harmonics Y_{mn}, used to describe the mountains satisfy $n \leq 21$ and $-n \leq m \leq n$). Due to the finite truncation, the actual minimum and maximum heights have somewhat different values. In the case of the table mountain the height reaches from a minimum of −121 m to a maximum of 1526 m. For the earth's mountains this was −606 m and 5488 m, respectively. Note that if the mountains η are represented spectrally by a TN truncation, $\tau = f\eta$ is represented spectrally by a TN + 1 truncation. So in the case of the Y_{33} orography, the N in Eq. (4) equals 4 and in the case of the table mountain and the earth's orography N equals 22. The pictures of the streamfunctions $\psi_f + \psi_\tau$ are dominated by easterlies, resulting from the Coriolis effect. Mountains show up as high streamfunction areas in the Northern Hemisphere. This is due to the vortex stretching effect of the mountains; on the Northern Hemisphere negative relative vorticity is introduced at the position of the mountains. The anomalous velocity fields introduced by these sources are superposed on the zonal easterlies. This is the effect of the orography in our model. So under the assumption

of constant potential vorticity in the tropical area, our model reproduces the prevailing easterlies in this region.

To obtain an expression for ψ_B we will use the technique of Green's functions, which gives rise to the typical contour dynamics calculations. We will summarize some of the definitions, which already appeared in VE, because we will need them for further calculations. The Green's function G of the Helmholtz operator $\nabla^2 - F$ is defined by the equation

$$\nabla^2 G(\mathbf{r};\mathbf{r}') - FG(\mathbf{r};\mathbf{r}') = \delta(\mathbf{r};\mathbf{r}), \quad (13)$$

and is given by (see VE)

$$G(\mathbf{r};\mathbf{r}') = -[4\cosh(\pi\kappa)]^{-1} P^0_{-1/2+i\kappa}(-\cos\theta''), \quad (14)$$

where $P^0_{-1/2+i\kappa}$ is a Legendre function with order 0 and complex degree $-1/2 + i\kappa$ as defined in Gradshteyn and Ryzhik (1965, their formula 8.840). These special Legendre functions are also known as conical functions. The parameter κ is related to F by $F = 1/4 + \kappa^2$. The argument $-\cos\theta''$, where θ'' is the angular distance between the points $\mathbf{r}$ and $\mathbf{r}'$, equals

$$\cos\theta'' = \sin\phi \sin\phi' + \cos\phi \cos\phi' \cos(\lambda - \lambda'). \quad (15)$$

It can be verified that due to (13) we have

$$\psi_B(\mathbf{r}) = \int_S G(\mathbf{r};\mathbf{r}') q_B(\mathbf{r}') dS' = (q_1 - q_0) \int_{R_1} G(\mathbf{r};\mathbf{r}') dS'. \quad (16)$$

Now it can be shown (see VE, appendix) that the Green's function can be written as a divergence:

$$G(\mathbf{r};\mathbf{r}') = \frac{1}{F}\left[\nabla'^2 V(\mathbf{r};\mathbf{r}') - \frac{1}{4\pi}\right], \quad (17)$$

which formula is also valid with the unaccented nabla operator, because $\nabla'^2 = \nabla^2$. Here V a scalar function defined by

$$V(\mathbf{r};\mathbf{r}') = G(\mathbf{r};\mathbf{r}') - H(\mathbf{r};\mathbf{r}'), \quad (18)$$

with

$$H(\mathbf{r};\mathbf{r}') \equiv \frac{1}{4\pi} \ln\left(\frac{1 - \cos\theta''}{2}\right). \quad (19)$$

Substituting (17) into (16) and using the divergence theorem, we obtain

$$\psi_B(\mathbf{r}) = -\frac{q_1 - q_0}{F}\frac{A_1}{4\pi} + \frac{q_1 - q_0}{F} \times \oint_B \mathbf{n}' \cdot \nabla' V(\mathbf{r};\mathbf{r}') dl', \quad (20)$$

where dl' is a line element along the boundary B and $\mathbf{n}'$ is a unit vector locally perpendicular to the boundary and to $\mathbf{k}$ and pointing away from R_1. By A_1 we denote the area of R_1.

The function H is the Green's function for the inversion of the barotropic potential vorticity, that is, the $F = 0$ case. It satisfies

$$\nabla^2 H(\mathbf{r};\mathbf{r}') + \frac{1}{4\pi} = \delta(\mathbf{r};\mathbf{r}'). \quad (21)$$

As for small scales and distances the equivalent barotropic equations reduce to the barotropic ones, H will equal the singularity in G. This observation allows us to interpret the function V as the desingularized Green's function. This property is advantageous in the numerical implementation of the formulas but from a theoretical point of view it is actually not necessary to introduce the function V. All formulas could as well be written in terms of G, thus complying more with the general literature on contour dynamics.

The velocity field follows from $\mathbf{v} = \mathbf{k} \times \nabla\psi$, where in view of (9), we can write

$$\nabla\psi = \nabla\psi_f + \nabla\psi_\tau + \nabla\psi_B. \quad (22)$$

The expressions for $\nabla\psi_f$ and $\nabla\psi_\tau$, can be derived straightforwardly from (11) and (12). For $\nabla\psi_B$, we can write [see (16)]

$$\nabla\psi_B(\mathbf{r}) = (q_1 - q_0) \int_{R_1} \nabla G(\mathbf{r};\mathbf{r}') dS'. \quad (23)$$

Now, also the gradient of the Green's function can be written in terms of a divergence (see VE, appendix):

$$\nabla G(\mathbf{r};\mathbf{r}') = \nabla' \cdot [G(\mathbf{r};\mathbf{r}')\mathsf{T}(\mathbf{r};\mathbf{r}')]. \quad (24)$$

This formula is valid for any function that is only dependent on the angular distance between $\mathbf{r}$ and $\mathbf{r}'$. The tensor T has a metrical nature and connects the gradient with respect to the variable $\mathbf{r}$ with that to the variable $\mathbf{r}'$. On a plane this tensor would be minus the identity but on the sphere it equals

$$\mathsf{T}(\mathbf{r};\mathbf{r}') \equiv -\frac{\cos\phi'}{\cos\phi}\mathbf{i}'\mathbf{i} + \sin\phi' \sin(\lambda - \lambda')\mathbf{i}'\mathbf{j} - \cos(\lambda - \lambda')\mathbf{j}'\mathbf{j}. \quad (25)$$

Substituting (24) into (23) and using the divergence theorem, we obtain

$$\nabla\psi_B(\mathbf{r}) = (q_1 - q_0) \times \oint_B \mathbf{n}' \cdot (G(\mathbf{r};\mathbf{r}')\mathsf{T}(\mathbf{r};\mathbf{r}'))dl'. \quad (26)$$

These expressions give the streamfunction and its gradient (and therefore the velocity) in terms of the boundary B. The last expression allows us to determine the evolution of B in terms of B itself. Each point of B

is advected by the velocity field at the corresponding point and this velocity is determined by the gradient of the streamfunction, as given by (22).

The contour dynamics system just described has two conserved quantities, the area A_1 enclosed by the contour and the total energy E_t,

$$A_1 = \int_{R_1} dS, \tag{27}$$

$$E_t = \frac{1}{2}\int_S [\mathbf{v}^2 + F\psi^2]dS. \tag{28}$$

(If the orography is zonally symmetric, then, in fact, also the total angular momentum is a conserved quantity.) In a contour dynamics context the conservation of patch area A_1 is the only one that remains of the infinite series of conserved quantities associated with the integrals of all possible functions of the potential vorticity, like, for example, the enstrophy. This can be best understood if one examines the true nature of this infinite series of conserved quantities. In fact, they follow from the conservation of all areas A_y of the subsets R_y of the sphere, which are defined as

$$R_y = \{\mathbf{r} \in S | q(\mathbf{r}) \leq y\}. \tag{29}$$

The areas of these sets are conserved if the q field is advected by any nondivergent velocity. Obviously, in our system the patch area is the only nontrivial area that is conserved.

Expressions (27) and (28) can be transformed into contour integrals. Using (21) we can rewrite the expression for the area, again using the divergence theorem, as

$$A_1 = -4\pi \int_{R_1} \nabla^2 H(\mathbf{r};\mathbf{r}')dS$$

$$= -4\pi \oint_B \mathbf{n}\cdot\nabla H(\mathbf{r};\mathbf{r}')dl, \tag{30}$$

if $\mathbf{r}'$ is chosen outside the region R_1. A convenient choice for this point is the south pole. The total energy E_t can also be written as a contour integral. In appendix A, we show that

$$E_t = E_b + E_{b,c} + E_c, \tag{31}$$

$$E_b = \frac{8\pi}{3(F+2)} + \frac{8\pi\tau_{01}}{\sqrt{3}(F+2)} + 2\pi\frac{\tau_{00}^2}{F} + 2\pi\sum_{n=1}^{N}\sum_{m=-n}^{n}\frac{\tau_{mn}^*\tau_{mn}}{F+n(n+1)}, \tag{32}$$

$$E_{b,c} = (q_1 - q_0)\oint_B \mathbf{n}\cdot\nabla(\chi_f + \chi_\tau)dl - \frac{4\pi\langle q\rangle\tau_{00}}{F}, \tag{33}$$

$$E_c = -\frac{(q_1 - q_0)^2}{2F} \times \oint_B\oint_B (\mathbf{nn}' : \mathsf{T}(\mathbf{r};\mathbf{r}'))V(\mathbf{r};\mathbf{r}')dldl' + \frac{4\pi\langle q\rangle^2}{2F}, \tag{34}$$

where

$$\chi_f = \frac{f}{2(F+2)}, \tag{35}$$

$$\chi_\tau = \sum_{n=1}^{N}\sum_{m=-n}^{n}\frac{\tau_{mn}}{n(n+1)[F+n(n+1)]}Y_{mn}. \tag{36}$$

Brackets $\langle g\rangle$, as in (33) and (34), denote the global average $(1/4\pi)\int_S g(\mathbf{r})dS$ of a scalar function g on the sphere. The area and the energy will be used to classify the stationary contours that will be considered in the next sections.

3. The case of no orography

In the absence of orography, zonal contours—that is, contours that coincide with a latitude circle—are stationary. This follows from the rotational symmetry of the system. Furthermore, linear Rossby wave perturbations on these contours have real phase velocities (see VE), which implies that zonal contours are linearly stable. The phase velocity of these waves is equal to the background velocity plus the Rossby wave velocity. The background velocity is the eastward velocity at the center of the jet, which is located at the contour. The Rossby wave velocity is westward and is caused by the self-advection of the wave. At certain parameter values these two contributions to the phase velocity can compensate each other, in which case the waves are stationary. These Rossby waves have the familiar feature that waves with the smallest wavenumbers have the largest Rossby wave velocities. For realistic zonal velocities, only small wavenumber (2, 3, 4) waves have a large enough Rossby wave velocity to compensate the background velocity. Small-scale perturbations, which have a relatively small Rossby wave velocity, are essentially advected eastward by the background velocity. More information about zonal contours and other stationary solutions in the absence of orography can be found in VE.

In Fig. 3 the energy of zonal contours is plotted against the area for $q_1 - q_0 = 2.81$. For this value of $q_1 - q_0$ a zonal contour at a latitude of 40° admits a stationary Rossby wave with wavenumber 4. Otherwise this choice for $q_1 - q_0$ is rather arbitrary in the sense that other values would lead to qualitatively the same picture. On the other hand, values of $q_1 - q_0 \approx 3$ lead to realistic peak velocities in the jet (see VE, Fig. 4). The energy and area in Fig. 3 are evaluated analytically.

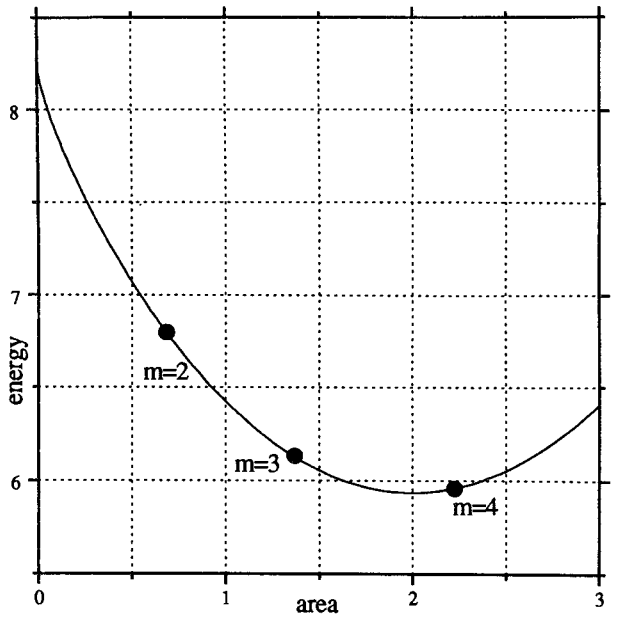

FIG. 3. The energy (in units 0.01) as a function of the area for zonal contours in the absence of orography. For the jump in potential vorticity we took $q_1 - q_0 = 2.81$, which is chosen such that the $m = 4$ resonance exactly lies at the contour with $\phi_B = 40°$. The calculations that lead to this plot are given in appendix B. The wavenumbers, plotted with the large dots, are the waves that are resonant at these points. The $m = 2$ wave is resonant on a zonal contour with latitude 62.7°, the $m = 3$ wave at 51.1°, and $m = 4$ wave at 40.0°.

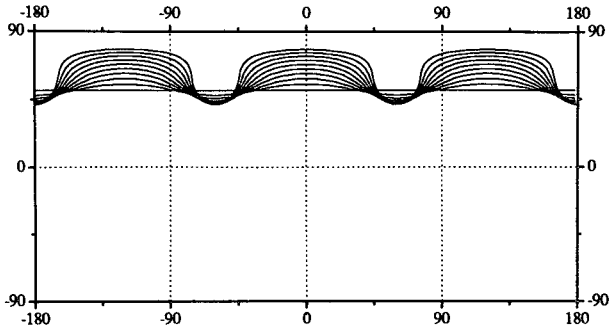

FIG. 4. A family of threefold symmetric finite-wave solutions, obtained by the method described in VE. The potential vorticity jump is $q_1 - q_0 = 2.81$, which is such that the zonal contour at $\phi_B = 51.1°$ supports a stationary $m = 3$ wave (see Fig. 3). This zonal contour is the first member in the family.

This calculation is presented in appendix B. In fact, we can interpret this plot as a two-dimensional projection of a part of phase space. That the energy has a minimum as a function of the patch area is due to the following effect: If the patch area is identically zero, the energy is the total energy in the westward velocity field produced by the Coriolis parameter. A small patch of high potential vorticity air around the north pole will introduce an eastward velocity around its boundary. This will compensate the westward background velocity, thus decreasing the total kinetic energy. Increasing the patch area, the energy will continue decreasing, until the kinetic energy of the eastward velocity field of the patch becomes higher than the kinetic energy in the background velocity field. From this point on the energy will start to increase as a function of area.

The large dots in Fig. 3 represent zonal contours that support stationary linear Rossby waves of the wavenumber that is plotted with the dots. At these points in phase space, the (at least) one-dimensional space of stationary contours, represented by the parabola-like line in Fig. 3, admits a second direction of stationary contours consisting of linear waves. In VE it is shown how these stationary linear perturbations can be extended numerically into the nonlinear finite-amplitude regime. In this way m-fold symmetric solutions with finite amplitude are obtained, starting from wavenumber m linear waves. These solutions are called "V states" [see Deem and Zabusky (1978), for planar geometry and Polvani and Dritschel (1993) for spherical geometry], though these more generally also include the rotating m-fold symmetric solutions. An example of a family of threefold symmetric solutions is given in Fig. 4. In Fig. 5 the energy and the area of these finite-amplitude solutions is plotted along with the energy and area of the zonal contours. We see how the wave solutions branch off from the zonal branch at the points where the corresponding linear waves are stationary. We will call these extra branches the "wave

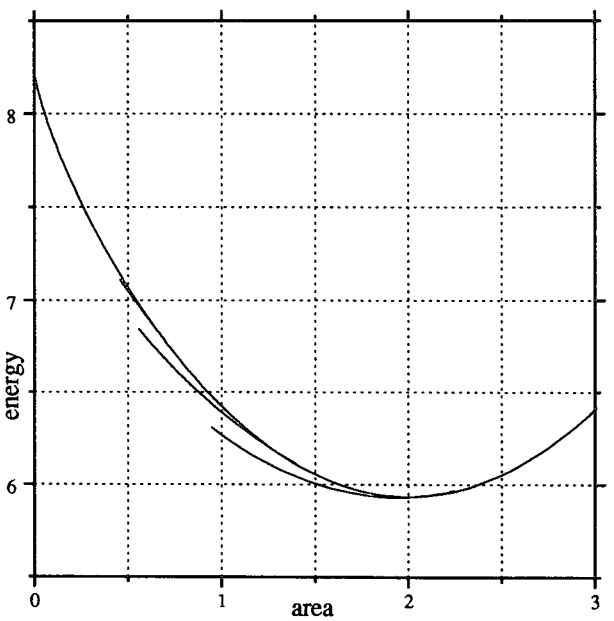

FIG. 5. As in Fig. 3, but now also the energy and area of the finite-wave solutions, as found by the method described in VE, are plotted. It is argued in section 4 that this is the phase portrait of stationary contours for vanishing orography.

branches." Note that the wave branches are themselves at least two-dimensional in the sense that the phase of these solutions is arbitrary. Because of the rotational symmetry, the phase does not influence the energy or the area.

As we can see from Fig. 5, the solutions organize themselves in lines on the energy–area graph. When we choose a point on any branch we see that there are at least two directions in phase space in which we find another stationary solution, namely along the branch in one or the other direction. These two directions correspond to a stationary linear perturbation that can be given a positive or negative amplitude. On the zonal branch an $m = 0$ perturbation is always stationary corresponding to a meridional shift of the zonal contour. On the wave branches a wavelike perturbation, with the same m-fold symmetry as the branch, is stationary.

Note also that the finite wave branches represent solutions that have an energy that is lower than the zonal solution with the same area. The question arises whether the zonal solutions are the maximum energy solutions for a given area. This question is of importance considering the possible nonlinear stability of zonal solutions. The general assertion, that zonal contours provide the maximum energy solutions for a given area does not hold. In fact, it is quite easy to find a contour for a given area that has a higher energy than the corresponding zonal contour. But these contours were arbitrary in the sense that they were not stationary. On the contrary, every *stationary* contour that we have found has a lower energy than the corresponding zonal contour. So the more specific assertion, that stationary solutions have energies lower than the energy of the zonal contour with the same area, might still be true. It remains to be proven though.

What changes in this picture of the phase space of stationary contours in the presence of orography is shown in the following sections. We will argue that there is a very clear correspondence between the phase spaces in the absence and in the presence of orography. Furthermore, we will find an important reinterpretation of the phase space of zonal contours by studying infinitesimal orography. This is the case we will consider in the next section. In a later section we will consider the finite-orography case.

4. Infinitesimal orography

Our next goal is to calculate stationary solutions in the presence of infinitesimal orography. This problem can be handled analytically. As a starting point let us again consider zonal contours. As before, they are stationary if the orography has zero height. A zonal contour, denoted by $\bar{B}$, is determined by its meridional position ϕ_B and can be parameterized by the longitude λ:

$$\bar{B} = \{(\lambda, \phi_B) | 0 \leq \lambda < 2\pi\}. \quad (37)$$

Now we will consider the orography to be $O(\epsilon)$, with $\epsilon \to 0$. The corresponding stationary contour will be a linearly perturbed zonal contour. We will assume that this perturbed contour can still be parameterized by the longitude, so we will assume that in the linear regime the contour is not a multivalued function of λ. Let us denote this perturbed contour, more or less abstractly, as $\bar{B} + \delta B$. So let us write

$$\bar{B} + \delta B = \{(\lambda, \phi_B + \delta\phi(\lambda)) | 0 \leq \lambda < 2\pi\}. \quad (38)$$

We will demand this contour to be stationary when the orography has the form

$$\tau = \epsilon(t_{00} + \sum_{n=1}^{N} \sum_{m=-n}^{n} t_{mn} Y_{mn}), \quad (39)$$

where $t_{mn} = O(1)$ when $\epsilon \to 0$. Because we write the orography in terms of spherical harmonics, it seems a judicious choice to write the corresponding contour perturbation $\delta\phi$ as a Fourier series in λ:

$$\delta\phi(\lambda) = \epsilon \sum_{m=-\infty}^{\infty} a_m e^{im\lambda}. \quad (40)$$

Here, $a_m = O(1)$ when $\epsilon \to 0$. So our problem can be stated as follows: calculate a_m such that the contour (38) is stationary in the presence of orography of the form (39).

The contour is stationary if the streamfunction is constant on the contour, because in this case the velocity perpendicular to the contour vanishes. The streamfunction ψ is a *function* of position $\mathbf{r}$ and a *functional* of the contour B [see (20)]. We will denote these dependencies in the total streamfunction as

$$\psi[B](\mathbf{r}).$$

So if our perturbed contour is stationary, we must have

$$\psi[(\lambda', \phi_B + \delta\phi(\lambda'))](\lambda, \phi_B + \delta\phi(\lambda)) = k, \quad (41)$$

where k must be constant as a function of λ. It can be expressed as a series expansion in ϵ:

$$k = k_0 + \epsilon k_1 + \epsilon^2 k_2 + \cdots. \quad (42)$$

Its zero-order term k_0 equals $\psi_0 + \psi_f + \psi_{\bar{B}}$ at latitude ϕ_B where $\psi_{\bar{B}}$ is evaluated for the zonal contour $\bar{B}$.

There are three first-order contributions to (41). First, there is the streamfunction ψ_τ due to the orography (39), which, because we are interested in first-order terms, can be evaluated at the original zonal contour's position. Then we have the first-order contribution to the streamfunction because $\psi_f + \psi_{\bar{B}}$ is evaluated at the new contour's position instead of the original zonal contour's position. This reflects the change of (41) due to the positional dependence of the contour's position. Finally, we have the streamfunction ψ_a, due to the anomaly potential vorticity δq, which is the difference in the q-field due to the change δB of the contour. Because we are interested in first-order effects,

this contribution can be evaluated at the original zonal contour's position. This contribution reflects the change of (41) due the functional dependence of the contour's position. Setting these three first-order terms equal to the first-order term in the constant in (41), we have

$$\psi_\tau(\lambda, \phi_B) + \frac{\partial(\psi_f + \psi_{\bar{B}})}{\partial\phi}(\lambda, \phi_B)\delta\phi(\lambda) + \psi_a(\lambda, \phi_B) = \epsilon k_1. \quad (43)$$

For the different terms on the left-hand side of (43), we have the following expressions:

$$\psi_\tau(\lambda, \phi_B) = \epsilon\left(\frac{t_{00}}{F} + \sum_{n=1}^{N}\sum_{m=-n}^{n}\frac{t_{mn}P_n^m(\sin\phi_B)e^{im\lambda}}{F + n(n+1)}\right), \quad (44)$$

$$\frac{\partial(\psi_f + \psi_{\bar{B}})}{\partial\phi}(\lambda, \phi_B)\delta\phi(\lambda) = -U_{\bar{B}}\delta\phi(\lambda) = -\epsilon\sum_{m=-\infty}^{\infty}U_{\bar{B}}a_m e^{im\lambda}, \quad (45)$$

$$\psi_a(\lambda, \phi_B) = \int_S G((\lambda, \phi_B); \mathbf{r}')\delta q(\mathbf{r}')dS', \quad (46)$$

where $U_{\bar{B}}$ is the zonal wind velocity at the contour's latitude due to the Coriolis parameter and the zonal potential vorticity patch. In appendix C we will show that the anomaly contribution (46) equals

$$\psi_a(\lambda, \phi_B) = -\epsilon\sum_{m=-\infty}^{\infty}c_m a_m e^{im\lambda}, \quad (47)$$

where c_m is the Rossby part of the wave velocity of a linear wave with wavenumber m (so the total wave velocity equals $U_{\bar{B}} + c_m$). Now observing that these three terms are all proportional to $e^{im\lambda}$, we can use the linear independence of complex exponentials to obtain

$$a_m = \sum_{n=|m|}^{N}\frac{t_{mn}}{F + n(n+1)}\frac{P_n^m(\sin\phi_B)}{U_{\bar{B}} + c_m} \quad \text{when} \quad 1 \leq m \leq N. \quad (48)$$

For $m > N$ the a_m vanish. The term a_0 is a function of k_1, which can be chosen such that a_0 also vanishes. This freedom expresses the fact that we can shift the basic zonal contour an amount proportional to ϵ without changing the wave amplitudes up to first order.

Equation (48) is the central result of this section. It has the familiar structure observed in formulas expressing the linear response of a barotropic model to orographic forcing. See, for example, Egger (1978, his formula 2.7). It expresses what amplitudes should be given to wavelike perturbations of the contour in order that their contributions to the streamfunction be exactly compensated by the streamfunction induced by the orography. Note that any Fourier component of the contour perturbation can only be compensated by the corresponding Fourier component of the orography. Note also that, when a component of the orography has a larger total wavenumber n, it has less influence on the corresponding stationary wave. This is of course the well known smoothing effect of the inversion operator, involved in obtaining the streamfunction from the potential vorticity (Hoskins et al. 1985). The amplitude of the wave a_m that meets the condition of stationarity is inversely proportional to it's total wave velocity. When the total wave velocity vanishes, the linear response is infinite. In fact, the wave will then saturate due to nonlinear effects. This is called a resonance. In Fig. 3 we can see which wave will be resonant at which position in phase space, the resonances corresponding to the large dots in the figure.

As we already mentioned, the mountains act as a source of negative relative vorticity, due to the vortex stretching effect. This results in an anticyclonic velocity field around the mountain. If the contour lies over the mountain, then at the east of the mountain the anticyclonic velocity will advect high potential vorticity air from the north to the south. But at the west of the mountain low potential vorticity air is advected northward (see Fig. 6). Now if the contour is perturbed by

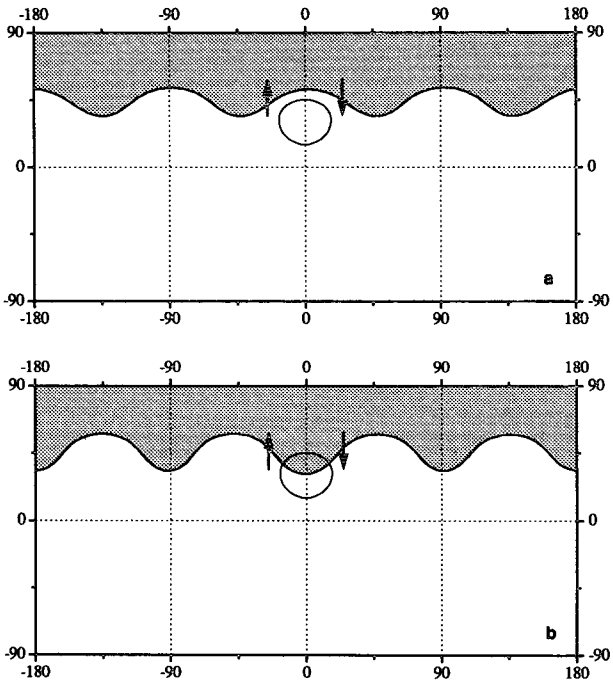

FIG. 6. In this picture the patch of high potential vorticity is shaded. A mountain at the position of the circle generates a negative vorticity, which induces a velocity field, as given by the arrows. In case (a) this velocity tends to advect the contour westward. In case (b) it tends to advect the contour eastward. Under the right conditions, as expressed by (48), this extra velocity can compensate for an opposite total wave velocity to make the wave stationary.

a wave with a ridge over the mountain (Fig. 6a), these advecting processes will tend to shift the wave westward. This extra velocity can, under the right circumstances [as expressed by (48)], compensate for an eastward total wave velocity, thus making the wave stationary. If a trough of the wave is over the mountain (Fig. 6b), the advection by the anticyclonic velocity will tend to shift the wave eastward, thus possibly compensating for a westward total wave velocity. This is the mechanism by which a mountain can make a wavelike perturbation on the contour stationary. From this mechanism it also becomes clear why a wave has to change sign if one passes through a resonance, thus changing the sign of the total wave velocity $U_{\bar{B}} + c_m$. More informally, one can think of the mountains producing Rossby waves on the contour. These will generally be radiated eastward, but due to the lack of friction the waves will circle the earth and meet the mountains again from the west with the original amplitude. Indeed, orography that is symmetric around a given longitude produces stationary waves that are also symmetric relative to this longitude. This can be easily deduced from (48). One can anticipate that inclusion of friction will introduce an eastward shift of the stationary waves, because, due to the damping of the Rossby waves circling the earth, most of the wave action is expected eastward of the mountains. A proper way of including forcing and friction into contour dynamics has not been established though.

In Fig. 7 we see how the response to infinitesimal orography, which is proportional to the orography from Fig. 2, changes when we pass from close to one resonance until over the next resonance. This is done by decreasing the latitude of the basic zonal contour, thus increasing the area of the patch. In fact, we follow the parabola-like line in Fig. 3 from close to one dot until over the next dot. We observe that close to a resonance the resonant wave dominates the stationary perturbation. In between two resonances we have a mixture of the two waves, except of course in the Y_{33} case, where only the $m = 3$ wave can be stationary. Passing through a resonance the wave indeed changes sign.

Now we will address the question of how the phase portrait in Fig. 3 changes on introducing infinitesimal orography. From (40) and (48) we see that, if we are not right on a resonance, the amplitude of the response will vanish if $\epsilon \to 0$. Thus, the phase portrait will not change at these points on introducing infinitesimal orography. At the resonant points though, the linear response will be infinite, irrespective of the magnitude of ϵ. So a zonal contour at a resonance is not a stationary solution when the amplitude of the orography goes to zero. In fact, the response will have a finite amplitude. Thus, we will arrive at the stationary finite wave solutions as found by VE, which are indeed stationary if the amplitude of the orography goes to zero. This leads us to the following conclusion: in the case of vanishing orography the phase portrait of stationary contours will look like Fig. 5 rather than Fig. 3. Otherwise formulated: for stationary contours, the limit of vanishing orography is a singular one.

5. Finite orography

In the previous sections we have discussed the changes that occur in the phase portrait of stationary waves when we introduce infinitesimal orography. We were able to find stationary solutions analytically in the presence of infinitesimal orography. These solutions consisted of infinitesimal perturbations of zonal contours. When the orography becomes finite this analytical treatment does not apply anymore. We can use numerical techniques to find stationary solutions in this case. In fact, we use the same numerical technique as described in VE, where it was used to find the finite amplitude waves mentioned in section 3. We obtain stationary solutions for the three types of orography displayed in Fig. 2: A simple Y_{33}-wave, a round table mountain, and the earth's orography.

The numerical procedure for finding stationary solutions in the nonlinear case is based on minimizing the functional

$$\mathcal{K} = \frac{1}{2}\int_a^b (\psi(\mathbf{r}(s)) - \psi_{\text{av}})^2 ds, \qquad (49)$$

where ψ_{av} is the average of the streamfunction over the contour B and s is a continuous label that parameterizes the contour. This functional $\mathcal{K}$ is positive except when the streamfunction is constant on the contour, which is again the condition for stationarity. In the numerical implementation of the method we represent the contour by a finite number of points (nodes) connected by pieces of great circle, a standard representation in contour dynamics. In our experiments the contour was usually represented by about 100 nodes. The contour integral in (20), involved in obtaining the streamfunction, and the one in (49) are replaced by a sum over the contour nodes. The minimization routine is a quasi-Newton algorithm from the NAG Fortran Library. Further details about the numerical implementation can be found in VE.

The convergence of the minimization procedure strongly depends on the quality of the first guess of the contour. The most successful method of obtaining good first guesses consisted in constructing families of stationary contours by linear extrapolation of both mountain height and contours. Suppose the $\mathbf{r}_i^{(n-1)}$ are the nodes, indexed by subscripts i, representing the stationary contour which we obtained by minimization of $\mathcal{K}$ at a mountain height $\eta^{(n-1)}$. The superscripts between round brackets label the members of a family. Suppose we also have the $\mathbf{r}_i^{(n)}$, obtained at a mountain height $\eta^{(n)}$. Now $\eta^{(n+1)}$ is taken as

$$\eta^{(n+1)} = \eta^{(n)} + (\eta^{(n)} - \eta^{(n-1)}). \qquad (50a)$$

A first guess of the points for the corresponding stationary contour is

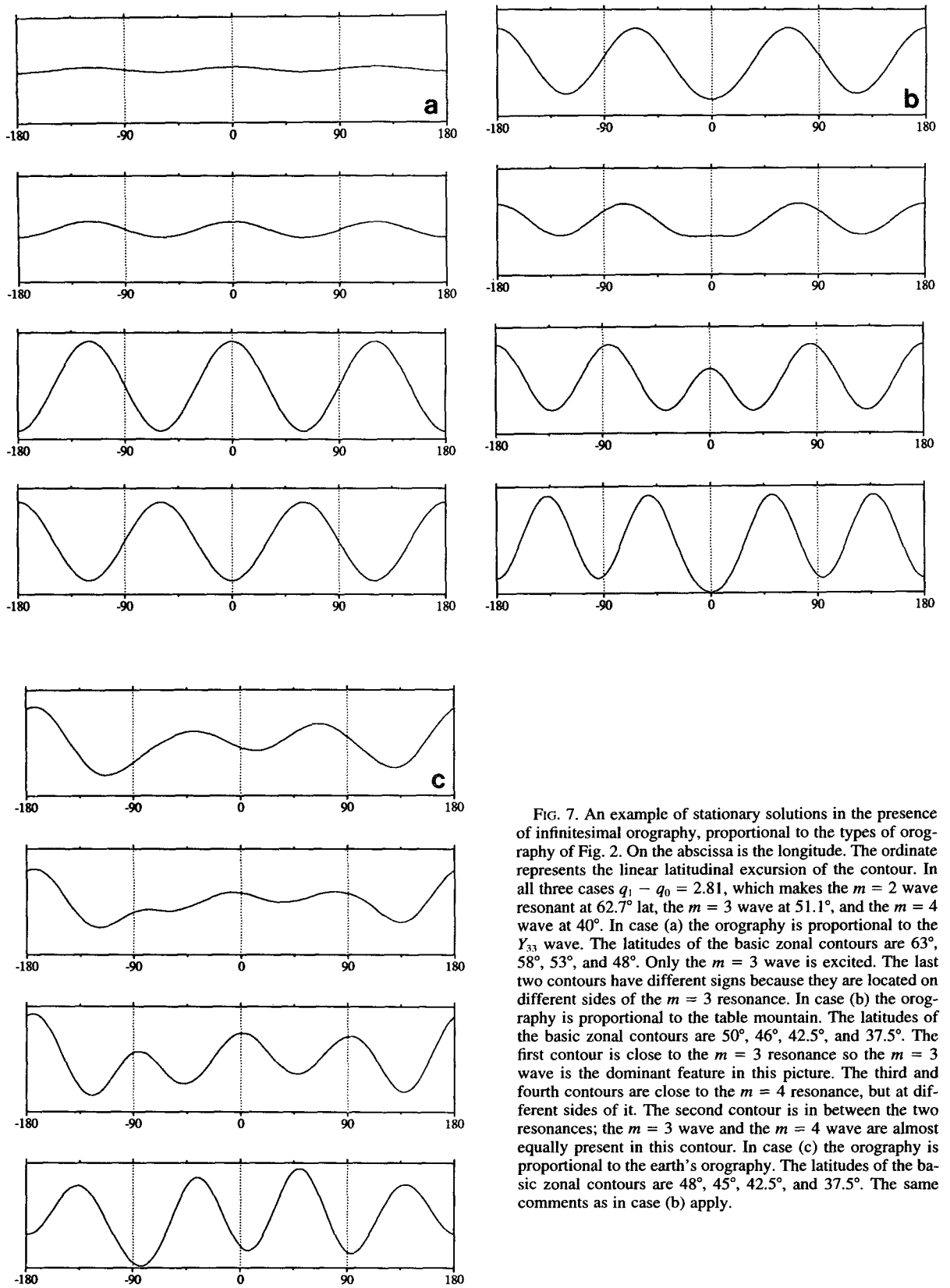

FIG. 7. An example of stationary solutions in the presence of infinitesimal orography, proportional to the types of orography of Fig. 2. On the abscissa is the longitude. The ordinate represents the linear latitudinal excursion of the contour. In all three cases $q_1 - q_0 = 2.81$, which makes the $m = 2$ wave resonant at 62.7° lat, the $m = 3$ wave at 51.1°, and the $m = 4$ wave at 40°. In case (a) the orography is proportional to the Y_{33} wave. The latitudes of the basic zonal contours are 63°, 58°, 53°, and 48°. Only the $m = 3$ wave is excited. The last two contours have different signs because they are located on different sides of the $m = 3$ resonance. In case (b) the orography is proportional to the table mountain. The latitudes of the basic zonal contours are 50°, 46°, 42.5°, and 37.5°. The first contour is close to the $m = 3$ resonance so the $m = 3$ wave is the dominant feature in this picture. The third and fourth contours are close to the $m = 4$ resonance, but at different sides of it. The second contour is in between the two resonances; the $m = 3$ wave and the $m = 4$ wave are almost equally present in this contour. In case (c) the orography is proportional to the earth's orography. The latitudes of the basic zonal contours are 48°, 45°, 42.5°, and 37.5°. The same comments as in case (b) apply.

$$\hat{\mathbf{r}}_i^{(n+1)} = \mathbf{r}_i^{(n)} + (\mathbf{r}_i^{(n)} - \mathbf{r}_i^{(n-1)}). \quad (50b)$$

Then starting from this first guess $\hat{\mathbf{r}}_i^{(n+1)}$, the minimization of $\mathcal{K}$ is applied, resulting in a new solution $\mathbf{r}_i^{(n+1)}$. In this fashion a family of stationary contours is constructed with ever higher mountains, where the last member corresponds to the desired (realistic) mountain height. As can be seen from (50b), we need two contours as starting points of the family. To this end we can work with a zonal contour, which is a stationary solution when the mountains have zero height. The second member of the family can be obtained by using this same zonal contour as a first guess for the minimization routine, which is well enough for small mountain heights. From these two contours we can start the construction of the family. Such a family we call a *primary family.*

If we construct two primary families that are the same except that the starting zonal contours are at a slightly different latitude, we find two final members at the same orography that are generally a little bit different from each other. These two contours can be used again as a starting point for an extrapolation scheme to construct another family but now at a constant mountain height. These families are called *secondary families.* In formulas the construction of a secondary family looks like

$$\eta^{(m+1)} = \eta^{(m)}, \quad (51a)$$

$$\hat{\mathbf{r}}_i^{(m+1)} = \mathbf{r}_i^{(m)} + (\mathbf{r}_i^{(m)} - \mathbf{r}_i^{(m-1)}). \quad (51b)$$

Then again starting from this first guess $\hat{\mathbf{r}}_i^{(m+1)}$, the minimization of $\mathcal{K}$ is applied, resulting in a new solution $\mathbf{r}_i^{(m+1)}$. So primary families consist of stationary contours with increasing mountain height, while secondary families consist of stationary contours at the same (generally finite) mountain height.

In Fig. 8 we depict some primary families obtained with the three types of orography. The height of the orography increases linearly through the family. The largest amplitude waves correspond to the highest orography and are the final members in the primary families. They are stationary at the mountain heights mentioned in Fig. 2. The potential vorticity discontinuity equals 2.81 in all three cases. It is noted that the solutions in Fig. 8a, which are stationary with mountains of the Y_{33} type, resemble the free solutions as found in VE (see Fig. 4). Notable differences though are that the amplitudes as well as the phases of the waves are not free parameters anymore. They are determined by the mountain's height and position.

In Fig. 9 some examples of secondary families are shown. The contours in one family are all stationary contours for the mountain heights in Fig. 2. Resonance features also play a role in the case of finite orography because some contours show little meridional structure while others have a strong dominant wave amplitude. On the other hand, resonance is only defined in the vanishing-orography case. One might say that resonance leaves a strong fingerprint in the nonlinear case. How this fingerprint looks like will become clear later in this section when we plot the energy–area graph of these stationary solutions.

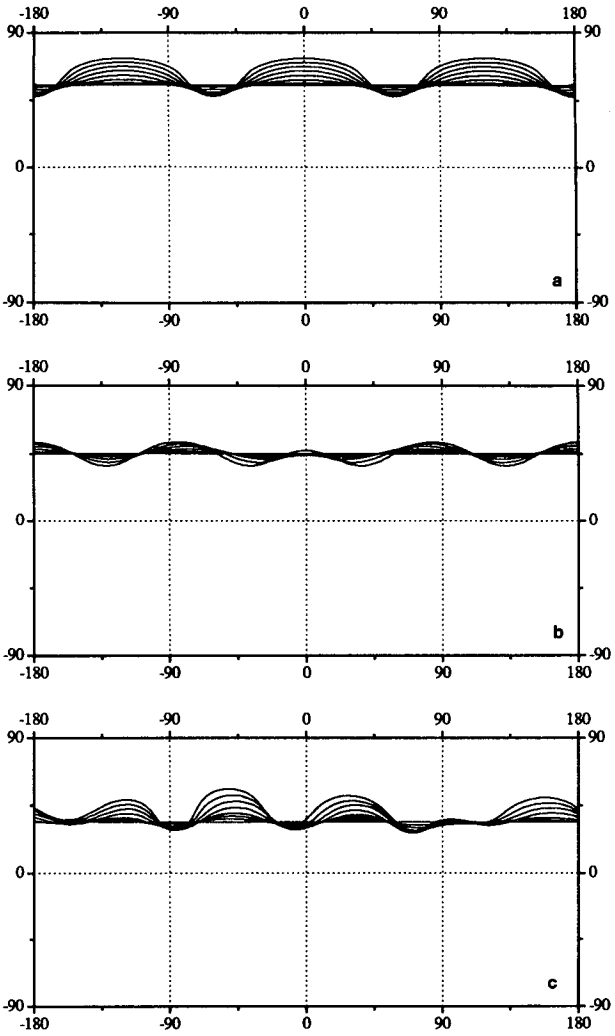

FIG. 8. Examples of primary families for orography, proportional to the three types of orography of Fig. 2. The constant by which the mountain height is multiplied varies in these families from 0 to 1. In all three cases $q_1 - q_0 = 2.81$.

In the construction of primary and secondary families a remarkable fact showed up: We found that the final members of primary families always coincide with some member of some secondary family. It also turned out that members of secondary families are always final members of some primary family. Moreover, we found that if we decreased the step size in the construction of the primary families—that is, if we let the height increase more slowly—the endpoint of the primary family, thus obtained, converged to a well-defined solution. This led us to conclude that *the construction of primary*

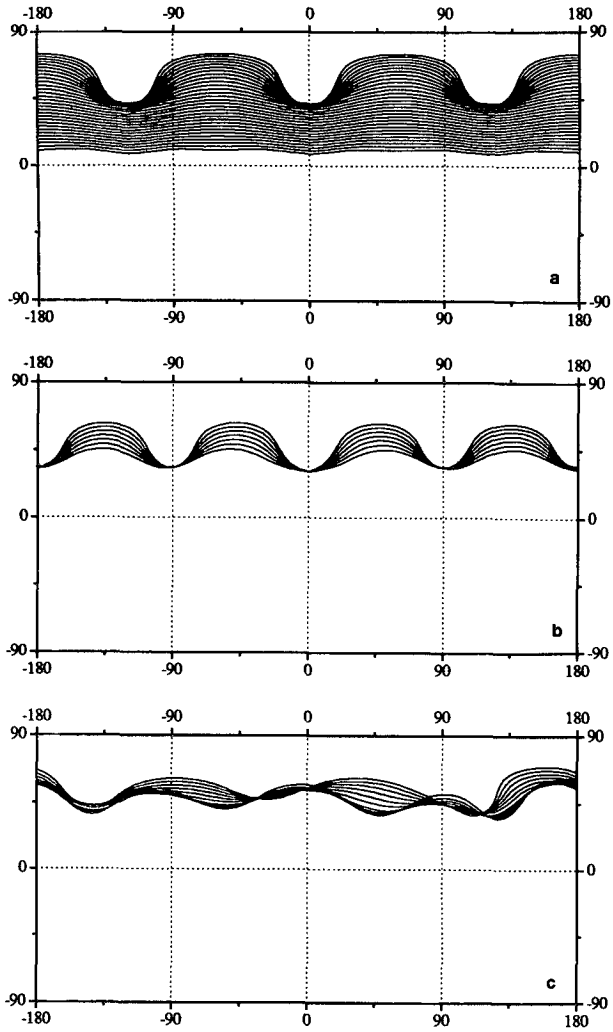

FIG. 9. Examples of secondary families of stationary contours for the three types of orography in Fig. 2. The heights of the mountains are constant in these families and equal to those in Fig. 2. In family (a) the area varied from 1.66 to 3.33, in family (b) from 1.99 to 2.59, in family (c) from 1.55 to 1.73.

families is a well-defined map of the zonal contours onto the stationary solutions with finite orography. This map is defined for any kind of orography and it maps a zonal contour onto a contour that is stationary at the given orography. The map is defined in theory for all zonal contours except for the resonant ones. In fact, not only at the resonances but already close to the resonances the map was difficult to find due to slow numerical convergence. In the same terminology we can call the treatment in the previous section the linearization of this map. This linearized map is defined explicitly by Eq. (48). Note that this linearized map is also not defined on resonances.

In Fig. 10 we plot the energy and the area of the solutions we found by our numerical technique for the three types of orography as displayed in Fig. 2. Because in the construction of a primary family one has to perform several minimizations to obtain the final member, while in the construction of secondary families only one minimization is needed to find this final member, the construction of secondary families is by far the most efficient way to obtain stationary solutions with a given finite orography. Therefore, most of the solutions in Fig. 10 are obtained as members of secondary families. Note that the energy–area graphs are divided into disconnected branches, every branch consisting of one secondary family. Let us describe how the graphs in Fig. 10 arise as images of Fig. 3 under the map defined above. If we increase the patch area of the zonal contour, we will generally find an increase of the area of its image under the map. The energy of the image will change accordingly. This correspondence explains the general parabola-like structure, which can be recognized in Fig. 10 as well as in Fig. 3. This correspondence though fails to hold if the zonal contour, by increasing it's area, comes close to a resonance. In this case, the image under the map will have a large wave amplitude, which reflects the resonance in the nonlinear case. But this large wave amplitude effectively decreases the area. This area decrease is seen as a cusp in the phase portrait. The extra branch one then finds we call the *first blocking branch* because it consists of stationary solutions with a strong wavelike character. When, on the other hand, we bring a zonal contour close to a resonance by decreasing its area, the image under the map again has a strong wavelike character, thus giving an even stronger decrease in the area. This branch of wavelike solutions we call the *second blocking branch.* The parts of the phase portrait that are not part of the first or second blocking branch we call the *zonal branch.* The solutions on the zonal branch have relatively low wave amplitude. An enlarged view of these branches around area 1.0 in Fig. 10c can be seen in Fig. 11. This structure is the generic fingerprint that resonance leaves in the nonlinear case. Note furthermore that the two blocking branches must converge to each other in the case of decreasing orography, until at vanishing orography they coincide as in Fig. 5.

As we can see in Fig. 10 and Fig. 11, the blocking branches have a finite length. At the contours at the end of the branches, which have a strong wavelike character, the construction of secondary families stops. This phenomenon is also present in the wave branches of Fig. 5. In VE it is speculated that this is the point where a topological transition from a single vorticity patch to multiple patches will start but that this transition cannot be reached because of limited resolution or that our method is simply not able to reach these transitions. On the other hand, the endpoints of the branches seem to be quite far from such a transition, and increasing the resolution did not bring us much further toward the topological transition. What precisely happens at these points remains a question of interest. The finiteness of

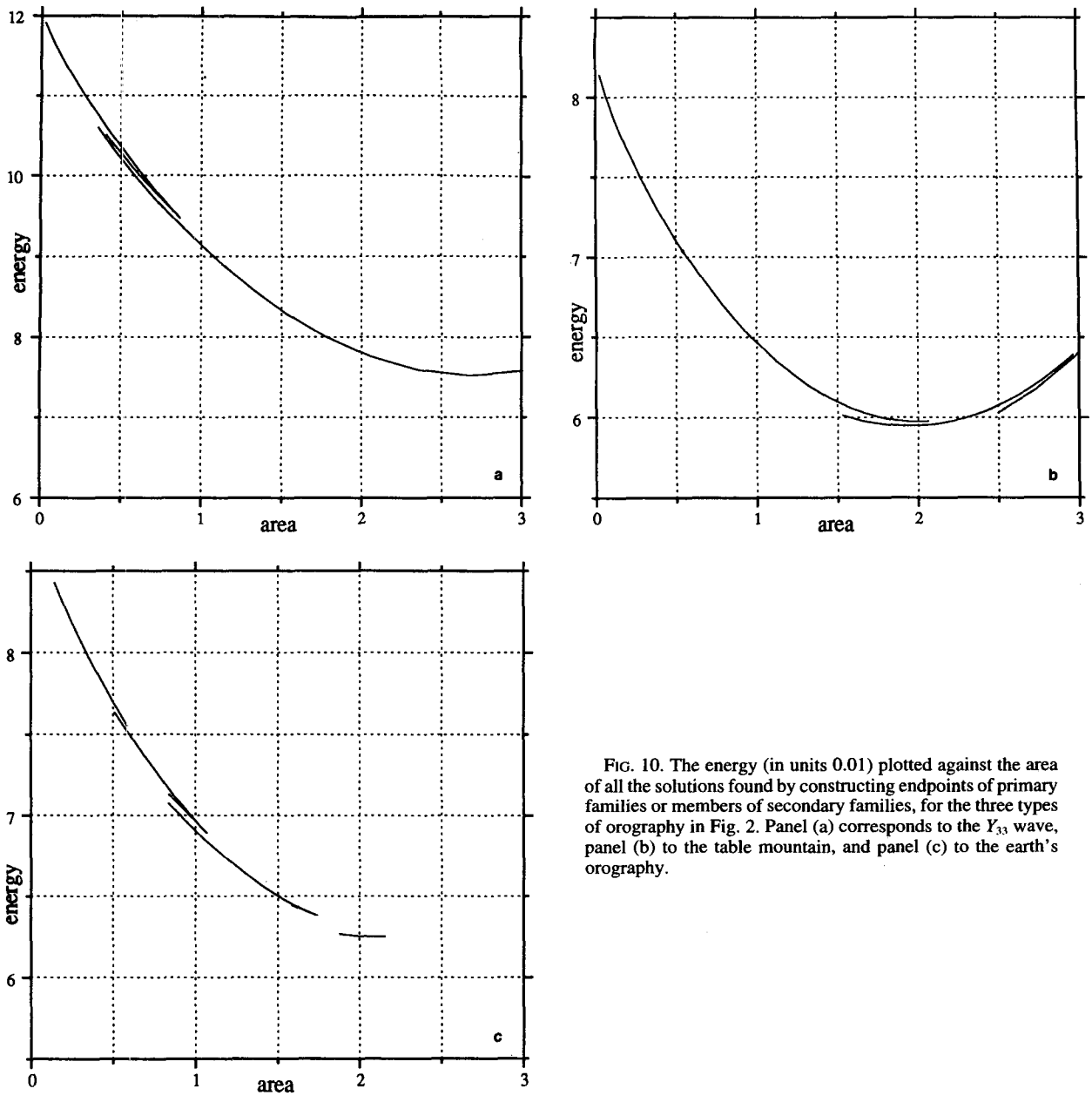

FIG. 10. The energy (in units 0.01) plotted against the area of all the solutions found by constructing endpoints of primary families or members of secondary families, for the three types of orography in Fig. 2. Panel (a) corresponds to the Y_{33} wave, panel (b) to the table mountain, and panel (c) to the earth's orography.

the branches has a definite effect on the structure of the energy–area graphs of Fig. 10. The branches can be so short that the generic picture of a resonance, as shown in Fig. 11, sometimes degenerates: the first blocking branch might be absent (as in the resonance around area 0.5 in Fig. 10c) or the zonal branch in between the second and first blocking branches is absent (as in the resonance-fragment around area 2 in Fig. 10c).

Because the first and second blocking branches are images, under the aforementioned map, of zonal contours that lie at different sides of one resonance, the corresponding wavelike solutions will be out of phase, as for the linearized map (see Fig. 7). To demonstrate these features we present in Fig. 12 the stationary solutions in the presence of the earth's orography for an area of 0.85. If we look at the phase portrait in Fig. 10c, or it's enlarged version in Fig. 11, we see that for this area there are three solutions that lie on the three different branches. Indeed, the two blocking-branch solutions are out of phase and have a large wave amplitude, contrary to the zonal-branch solution. Note furthermore that, though the structure of the three solutions is completely different, their areas are identical and their energies differ by only a small amount. Here we have in a sense the unforced and undamped analog of the multiple steady-state solutions due to the orog-

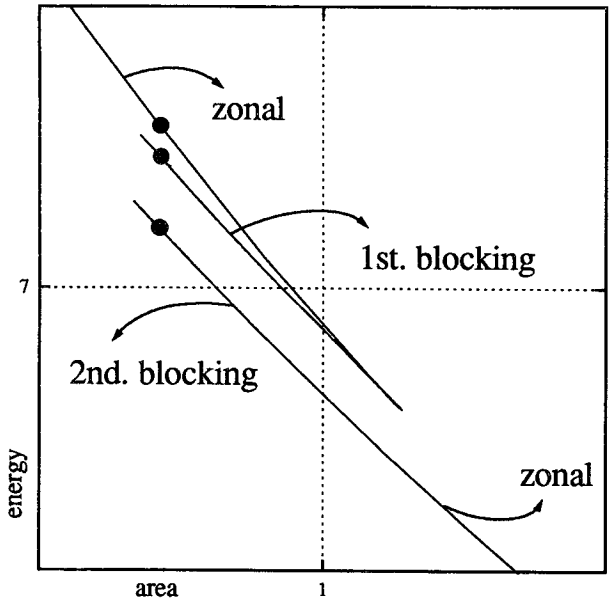

FIG. 11. Enlarged view of the part of Fig. 10c around area 1.0. This picture is the generic structure of the fingerprint that resonance leaves in the nonlinear case. It shows the three branches close to a resonance. The large dots in the figure represent solutions with an area of 0.85. They are depicted in Fig. 12.

raphy. In the forced and damped case this was first observed in a study of Charney and DeVore (1979). These results have been reproduced since then by a number of authors, but always in the context of models with relatively few degrees of freedom and simple orography. Here we observe an analogous behavior in a contour dynamics model, which has substantially more degrees of freedom, and realistic orography. Identifying regimes with stationary solutions of a model, we are able to find a number of qualitatively very distinct regimes that are very close to each other in terms of their energy and area.

6. Summary and outlook

In this article we investigated the effect of mountains in a contour dynamics model of large-scale atmospheric flow. This seems to be both a natural and necessary extension of the "free" dynamics, as presented in VE. The research was centered upon finding stationary solutions. The mountains, as well as the Coriolis effect, are described by an effective additional streamfunction. The flow induced by this additional streamfunction is dominated by easterlies, resulting from the Coriolis effect, disturbed by relative highs, resulting from the orography (Fig. 2).

First, the linear case was considered. Here the mountain heights are taken to be infinitesimal, as well as the contour's latitudinal excursion. It followed that for every orography a stationary contour could be found except when the induced wavelike contour disturbance had a zero total wave velocity. The latter situation is called a resonance. In all other cases every Fourier component of the orography induced a corresponding Fourier component in the contour's perturbation (Fig. 7).

Actually, the limit for vanishing mountain heights is a singular one. The picture of the zonal contours as the stationary solutions to the model without orography is not robust in the sense that any infinitesimal orographic forcing will blow up the resonant contours up to a finite-amplitude wave. These finite-amplitude waves are the free modes as found in VE. In an energy–area graph, where the energy is plotted as a function of the patch area, this singular limit can be seen as an extra branch that springs from the branch of zonal contours at the points of resonance (Fig. 5).

When the orography is made finite, this extra branch splits into two branches representing wavelike contours that are out of phase. The phases of the branches are determined by the mountain's position. These branches are called the blocking branches because they exhibit a strong wavelike character with large meridional excursions of the contour. These contours were found by an iterative process where we minimized a functional that measures the distance from stationarity. By extrapolation of different solutions with a finite mountain height, we gained a quite complete picture of the possible stationary solutions of the problem with orography. They form a one-dimensional set, which is piecewise connected. Resonances leave a strong fingerprint in the nonlinear case. Close to such a resonance we generally find three solutions that have the same area but a slightly different energy, analogous to the multiple steady-state solutions with orography, found by other authors.

The search of stationary solutions is inspired by the fact that they might be identified with regimes. Our contour dynamics model of the large-scale atmospheric flow is capable of reproducing stationary solutions that are realistic, both concerning their amplitudes and their phases. Blocked as well as zonal solutions are obtained. The solutions are organized in one-dimensional piecewise connected sets, which might serve as a catalog of regimes.

The question of stability of the solutions is still an open one and is currently under investigation. Preliminary time integrations show that the stationary solutions retain their structure for at least 10–20 days. To prove nonlinear or formal stability analytically, usually Lyapunov functionals are introduced involving combinations of energy, Casimirs, and other conserved quantities. As non–zonally symmetric orography breaks the rotational symmetry of the system, angular momentum is not a conserved quantity anymore. This broken symmetry will probably make the system even less tractable to analytical proofs of stability. The problem of introducing forcing and friction in contour dy-

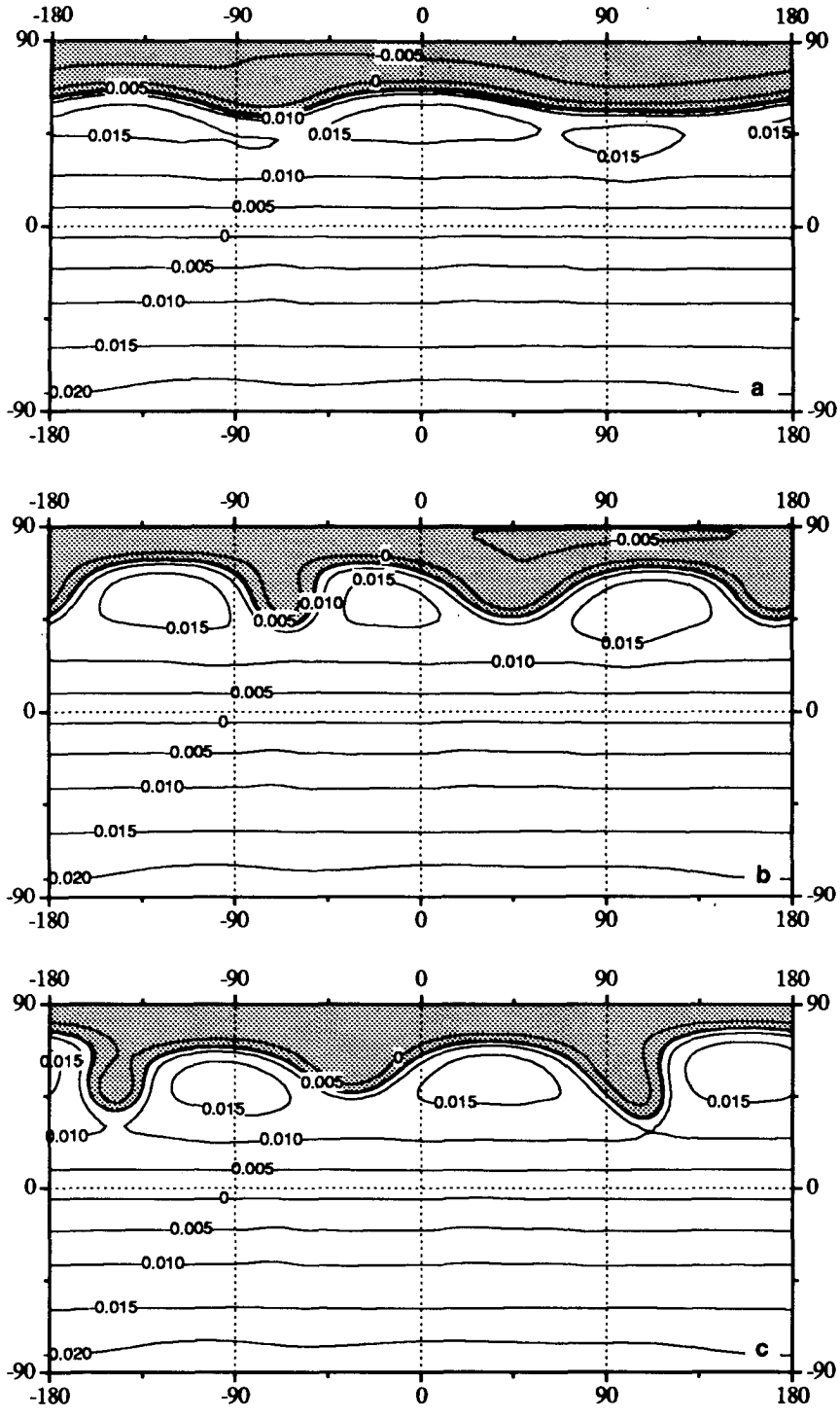

FIG. 12. Three stationary solutions in the presence of the earth's orography. Shaded are the vorticity patches. The streamlines are also drawn. The boundary of the patches coincide with a streamline, which means that they are stationary solutions. All three solutions have an area of 0.85 (see Fig. 11). Contour (a) is on the zonal branch, (b) on the first blocking branch, and (c) on the second blocking branch.

namics, which is essentially nonviscous, poses another challenge. Once this problem has been solved, we can investigate the robustness of the solutions under forcing and friction.

Acknowledgments. We thank the anonymous reviewers for their helpful comments. This work was partially supported by the Netherlands Geosciences Foundation (GOA), with financial aid from the Netherlands Organization for Scientific Research (NWO).

APPENDIX A

Energy of the Patch in Terms of a Contour Integral

Using the definition of the streamfunction, we can rewrite (28) as

$$E_t = \frac{1}{2}\int_S [\nabla\psi(\mathbf{r})\cdot\nabla\psi(\mathbf{r}) + F\psi(\mathbf{r})^2]dS. \quad \text{(A1)}$$

Applying the divergence theorem we can write this as

$$E_t = -\frac{1}{2}\int_S \psi(\mathbf{r})(\nabla^2 - F)\psi(\mathbf{r})dS$$

$$= -\frac{1}{2}\int_S \psi(\mathbf{r})(q - f - \tau)(\mathbf{r})dS, \quad \text{(A2)}$$

where (8) is used. Using the Green's function G, we can rewrite ψ in terms of the potential vorticity, by inverting equation (8):

$$E_t = -\frac{1}{2}\int_S\int_S (q - f - \tau)(\mathbf{r})G(\mathbf{r};\mathbf{r}')$$

$$\times (q - f - \tau)(\mathbf{r}')dSdS' = E_b + E_{b,c} + E_c, \quad \text{(A3)}$$

where

$$E_b = -\frac{1}{2}\int_S\int_S (f + \tau)(\mathbf{r})G(\mathbf{r};\mathbf{r}')$$

$$\times (f + \tau)(\mathbf{r}')dSdS', \quad \text{(A4)}$$

$$E_{b,c} = \int_S\int_S q(\mathbf{r})G(\mathbf{r};\mathbf{r}')(f + \tau)(\mathbf{r}')dSdS', \quad \text{(A5)}$$

$$E_c = -\frac{1}{2}\int_S\int_S q(\mathbf{r})G(\mathbf{r};\mathbf{r}')q(\mathbf{r}')dSdS'. \quad \text{(A6)}$$

The term E_b as given by (A4) is the energy in the background field as produced by the earth's rotation and the orography. It is independent of the q field. Its value can be obtained quite easily if one interprets the integration over $\mathbf{r}'$ as the inversion of the Helmholtz operator $(\nabla^2 - F)$. As both f and τ are given in spherical harmonics, which are eigenfunctions of the Helmholtz operator, this inversion is straightforward. See formulas (11) and (12). Using the orthogonality relation (5) for spherical harmonics, the integration over $\mathbf{r}$ also becomes straightforward. The result is given in (32).

The second term (A5) represents the energy following from the interaction of the q field with the background field. The integration over $\mathbf{r}'$ can again be interpreted as the inversion of the Helmholtz operator. Performing this inversion we can rewrite (A5) as

$$E_{b,c} = -\int_S q(\mathbf{r})(\psi_f + \psi_\tau)(\mathbf{r})dS = (q_1 - q_0)$$

$$\times \oint_B \mathbf{n}\cdot\nabla(\chi_f + \chi_\tau)(\mathbf{r})dl - \frac{4\pi\langle q\rangle\tau_{00}}{F}, \quad \text{(A7)}$$

where the divergence theorem is used again and χ_f and χ_τ are such that

$$\nabla^2\chi_f = -\psi_f \quad \text{and} \quad \nabla^2\chi_\tau = \frac{\tau_{00}}{F} - \psi_\tau. \quad \text{(A8)}$$

The fields $-\psi_f$ and $\tau_{00}/F - \psi_\tau$ are given in spherical harmonics and their global average vanishes. So the inversion of the Laplace operator in (A8) becomes straightforward and unique. The results of this inversion are in (35) and (36).

The third term (A6) represents the self-energy of the q field, which would be the only contribution to the energy in the absence of planetary vorticity or orography. Using (17) without the accent on the nabla operator we can write

$$E_c = -\frac{1}{2F}\int_S\int_S q(\mathbf{r})$$

$$\times \left[\nabla^2 V(\mathbf{r};\mathbf{r}') - \frac{1}{4\pi}\right]q(\mathbf{r}')dSdS'. \quad \text{(A9)}$$

Then we apply (24), which is also valid for V, because this is also a function of the angular distance between $\mathbf{r}$ and $\mathbf{r}'$:

$$E_c = -\frac{1}{2F}\int_S\int_S q(\mathbf{r})[\nabla\cdot(\nabla'\cdot(V(\mathbf{r};\mathbf{r}')\mathsf{T}(\mathbf{r};\mathbf{r}')))]$$

$$\times q(\mathbf{r}')dSdS' + \frac{1}{2F}\frac{1}{4\pi}\left(\int_S q(\mathbf{r})dS\right)^2. \quad \text{(A10)}$$

Finally, we use the divergence theorem to obtain

$$E_c = -\frac{(q_1 - q_0)^2}{2F}\oint_B\oint_B (\mathbf{nn}' : \mathsf{T}(\mathbf{r};\mathbf{r}'))$$

$$\times V(\mathbf{r};\mathbf{r}')dldl' + \frac{4\pi\langle q\rangle^2}{2F}. \quad \text{(A11)}$$

For this derivation the remark under formula (21) also applies: the formulas could evenly well be rewritten in terms of G instead of V, using (13) instead of (17). Thus, we arrive at an equivalent formulation in terms

of G instead of V, which we state for the sake of completeness:

$$E_c = -\frac{(q_1 - q_0)^2}{2F}\oint_B\oint_B (\mathbf{nn}' : \mathsf{T}(\mathbf{r}, \mathbf{r}')) \times G(\mathbf{r}, \mathbf{r}')dldl' + \frac{4\pi\langle q^2\rangle}{2F}. \quad \text{(A12)}$$

Note that, apart from the use of V or G, the only difference between (A11) and (A12) is the relative position of the square to the averaging brackets. In the actual numerical implementation of these formulas, we used (A11), which is more appropriate because here one does not integrate over a singularity. In analytical calculations equation (A12) is usually more appropriate (cf. appendix B).

APPENDIX B

Energy of a Zonal Patch without Orography

When the potential vorticity patch is zonal, the calculation of the energy can be done explicitly. We will do this calculation in the absence of orography in order to obtain the graph in Fig. 3. The abscissa of this graph is the area A_1 of the zonal patch. It can be obtained easily and equals

$$A_1 = 2\pi(1 - \sin\phi_B), \quad \text{(B1)}$$

where ϕ_B is the latitude of the boundary B.

The energy E_t contains three contributions as in (31). The first contribution to (31) is (32). Its evaluation in the absence of orography is easy:

$$E_b = \frac{8\pi}{3(F + 2)}. \quad \text{(B2)}$$

In the second contribution (33) again the terms with orography vanish. The resulting contour integral can be performed easily for a zonal contour. Note that the unit normal vector on the contour equals $-\mathbf{j}$. So we arrive at

$$E_{b,c} = (q_1 - q_0)\oint_{\bar{B}} \mathbf{n}\cdot\nabla\chi_f dl = (q_1 - q_0)\int_0^{2\pi} -\frac{\partial}{\partial\phi}\left(\frac{f}{2(F + 2)}\right)\cos\phi_B d\lambda = -\frac{2\pi(q_1 - q_0)\cos^2\phi_B}{F + 2}. \quad \text{(B3)}$$

To evaluate the last contribution (34) for a zonal contour, we use formula (A12), which is equivalent to (A11) or (34). First we have

$$\frac{4\pi\langle q^2\rangle}{2F} = \frac{4\pi}{2F}\frac{1}{4\pi}[q_1^2 A_1 + q_0^2(4\pi - A_1)] = \frac{\pi}{F}[q_1^2(1 - \sin\phi_B) + q_0^2(1 + \sin\phi_B)]. \quad \text{(B4)}$$

In order to evaluate the contour integral in (A12) for a zonal patch we must contract the T tensor first with $-\mathbf{j}'$ and then with $-\mathbf{j}$. This equals $-\cos(\lambda - \lambda')$. So we have, using (14),

$$\oint_B\oint_B (\mathbf{nn}' : \mathsf{T}(\mathbf{r}; \mathbf{r}'))G(\mathbf{r}; \mathbf{r}')dldl' = \int_0^{2\pi}\int_0^{2\pi}\cos(\lambda - \lambda')\frac{1}{4\cosh(\pi\kappa)} \times P^0_{-1/2+i\kappa}(-\cos\theta'')\cos^2\phi_B d\lambda d\lambda', \quad \text{(B5)}$$

where [see (15)]

$$\cos\theta'' = \sin^2\phi_B + \cos^2\phi_B\cos(\lambda - \lambda'). \quad \text{(B6)}$$

At this point we have to introduce the addition theorem for Legendre functions. It can be found in Gradshteyn and Ryzhik (1965) in several equivalent forms. We will use their formula 8.796 in combination with 8.752.2. Furthermore, we use the fact that the change of variables $\phi \to \phi - \pi/2$ changes $\cos\phi$ into $\sin\phi$ and vice versa. So for our purposes we can state the addition theorem as

$$P^0_\nu(-\sin\psi_1\sin\psi_2 - \cos\psi_1\cos\psi_2\cos\xi) = P^0_\nu(-\sin\psi_1)P^0_\nu(\sin\psi_2) + 2\sum_{m=1}^{\infty}(-1)^m\frac{\Gamma(\nu - m + 1)}{\Gamma(\nu + m + 1)}P^m_\nu(-\sin\psi_1) \times P^m_\nu(\sin\psi_2)\cos m\xi, \quad \text{(B7)}$$

where $-\pi/2 < \psi_1 < \psi_2 < \pi/2$ and ξ is real. In our case the theorem is also defined for $\psi_1 = \psi_2$. Note that if we take $\nu = -1/2 + i\kappa$ and $\psi_1 = \psi_2 = \phi_B$ and $\xi = \lambda - \lambda'$, the addition theorem precisely matches the form of the integrand in (B5), up to a factor. Now using the addition theorem in (B5), we see that the integrations over λ and λ' become trivial: the only nonvanishing contribution is the $m = 1$ term in (B7) and we arrive at

$$\int_0^{2\pi}\int_0^{2\pi}\cos(\lambda - \lambda')\frac{1}{4\cosh(\pi\kappa)}P^0_{-1/2+i\kappa}(-\cos\theta'') \times\cos\phi_B^2 d\lambda d\lambda' = -\frac{\pi^2}{\cosh(\pi\kappa)} \times\frac{\Gamma(-1/2 + i\kappa)}{\Gamma(1/2 + i\kappa + 2)}P^1_{-1/2+i\kappa}(-\sin\phi_B) \times P^1_{-1/2+i\kappa}(\sin\phi_B)\cos^2\phi_B. \quad \text{(B8)}$$

Using $\Gamma(x + 1) = x\Gamma(x)$ and $F = 1/4 + \kappa^2$, we can further simplify this

$$\frac{\Gamma(-1/2 + i\kappa)}{\Gamma(1/2 + i\kappa + 2)} = -\frac{1}{F}. \quad \text{(B9)}$$

Now we can write down the complete expression for the energy of a zonal contour in the absence of orography:

$$E_t = E_b + E_{b,c} + E_c = \frac{8\pi}{3(F+2)} - \frac{2\pi(q_1 - q_0)\cos^2\phi_B}{F+2} + \frac{\pi}{F}[q_1^2(1 - \sin\phi_B) + q_0^2(1 + \sin\phi_B)] - \frac{(q_1 - q_0)^2}{2F^2}\frac{\pi^2}{\cosh(\pi\kappa)} \times P^1_{-1/2+i\kappa}(-\sin\phi_B)P^1_{-1/2+i\kappa}(\sin\phi_B)\cos^2\phi_B. \quad \text{(B10)}$$

This is a function of ϕ_B. As the area A_1 is a monotonous function of ϕ_B, we can also write the energy as a function of the area. This dependence is plotted in Fig. 3.

APPENDIX C

Streamfunction Due to a Linear Perturbation

In this appendix we will evaluate the anomaly streamfunction ψ_a, as given in (46). First, we will evaluate its value for the whole sphere and later we will relate its value on the zonal contour to the Rossby wave velocity c_m, as in (47).

So we have, using (46)

$$\psi_a(\mathbf{r}) = \int_S G(\mathbf{r};\mathbf{r}')\delta q(\mathbf{r}')dS' = (q_1 - q_0)\oint_{\bar{B}} \mathbf{n}'\cdot\delta\mathbf{r}'G(\mathbf{r};\mathbf{r}')dl' = -(q_1 - q_0)\int_0^{2\pi}\delta\phi(\lambda') \times G(\lambda, \phi; \lambda', \phi_B)\cos\phi_B d\lambda', \quad \text{(C1)}$$

where we have used $\mathbf{n}\cdot\delta\mathbf{r} = -\delta\phi(\lambda)$ as in (38). Now we can substitute (40) for $\delta\phi(\lambda)$ and we can rewrite this formula as follows by using that $G(\lambda, \phi; \lambda', \phi_B)$ is a function of $\lambda - \lambda'$:

$$\psi_a(\lambda, \phi) = (q_1 - q_0)\epsilon \sum_{m=-\infty}^{\infty} \chi_m(\phi, \phi_B)a_m e^{im\lambda}, \quad \text{(C2)}$$

where

$$\chi_m(\phi, \phi_B) = \cos\phi_B \int_0^{2\pi} G(\lambda, \phi; \lambda', \phi_B) \times e^{-im(\lambda-\lambda')}d(\lambda - \lambda'). \quad \text{(C3)}$$

In fact, C1 is a convolution of $\delta\phi$ and G. But a convolution equals a product in Fourier space as in (C2). As $G(\lambda, \phi; \lambda', \phi_B)$ is an even function of $\lambda - \lambda'$, we can rewrite (C3) as

$$\chi_m(\phi, \phi_B) = \cos\phi_B \int_0^{2\pi} G(\lambda, \phi; \lambda', \phi_B) \times \cos m(\lambda - \lambda')d(\lambda - \lambda') = \frac{-\cos\phi_B}{4\cosh(\pi\kappa)}\int_0^{2\pi} P^0_{-1/2+i\kappa}(-\sin\phi\sin\phi_B - \cos\phi\cos\phi_B\cos(\lambda - \lambda')) \times \cos m(\lambda - \lambda')d(\lambda - \lambda'), \quad \text{(C4)}$$

where for the last equality the definition of the Green's function is used. The integrand meets the form of the addition theorem (B7) up to a factor and using this theorem, the integration over $(\lambda - \lambda')$ becomes trivial. According to the constraints of the addition theorem we must distinguish between $\phi \leqslant \phi_B$ and $\phi \geqslant \phi_B$. For $\phi \leqslant \phi_B$ we find

$$\chi_m(\phi, \phi_B) \overset{\phi\leqslant\phi_B}{=} -\frac{2\pi(-1)^m\cos\phi_B}{4\cosh(\pi\kappa)} \times \frac{\Gamma(1/2 + i\kappa - m)}{\Gamma(1/2 + i\kappa + m)} P^m_{-1/2+i\kappa}(-\sin\phi) \times P^m_{-1/2+i\kappa}(\sin\phi_B), \quad \text{(C5)}$$

while for $\phi \geqslant \phi_B$ we have

$$\chi_m(\phi, \phi_B) \overset{\phi\geqslant\phi_B}{=} -\frac{2\pi(-1)^m\cos\phi_B}{4\cosh(\pi\kappa)} \times \frac{\Gamma(1/2 + i\kappa - m)}{\Gamma(1/2 + i\kappa + m)} P^m_{-1/2+i\kappa}(-\sin\phi_B) \times P^m_{-1/2+i\kappa}(\sin\phi). \quad \text{(C6)}$$

At $\phi = \phi_B$ these expressions coincide. These expressions for χ_m should be compared with the expressions for χ in VE with the identification

$$\chi(\phi) = \chi_m(\phi, \phi_B) \quad \text{(C7)}$$

[see VE, Eq. (50)]. A fair amount of manipulations, involving the Wronskian of two Legendre functions, prove that these expressions for χ are equivalent to the more involved expressions derived in VE.

In VE is also shown that

$$-(q_1 - q_0)\chi_m(\phi_B, \phi_B) = c_m, \quad \text{(C8)}$$

[cf. VE, Eq. (60)]. Here we have defined the Rossby wave velocity c_m as the difference between the total phase velocity of a wave with wavenumber m and the zonal velocity $U_{\bar{B}}$. Now, combining (C2) and (C8), we have

$$\psi_a(\lambda, \phi_B) = \epsilon \sum_{m=-\infty}^{\infty} c_m a_m e^{im\lambda}, \quad \text{(C9)}$$

where, combining (C8) and (C5) or (C6), we have

$$c_m = (q_1 - q_0)\frac{2\pi(-1)^m}{4\cosh(\pi\kappa)}\frac{\Gamma(1/2 + i\kappa - m)}{\Gamma(1/2 + i\kappa + m)} \times P^m_{-1/2+i\kappa}(-\sin\phi_B)P^m_{-1/2+i\kappa}(\sin\phi_B). \quad \text{(C10)}$$

REFERENCES

Bolin, B., 1950: On the influence of the earth's orography on the general character of the westerlies. *Tellus,* **2,** 184–195.

Charney, J. G., and A. Eliassen, 1949: A numerical method for predicting the perturbations of the middle latitude westerlies. *Tellus,* **1,** 38–54.

——, and J. G. DeVore, 1979: Multiple flow equilibria in the atmosphere and blocking. *J. Atmos. Sci.,* **36,** 1205–1206.

Deem, G. S., and N. J. Zabusky, 1978: Vortex waves: Stationary "V-states," interactions, recurrence, and breaking. *Phys. Rev. Lett.,* **40,** 859–862.

Dritschel, D. G., 1985: Stability and energetics of corotating uniform vortices. *J. Fluid Mech.,* **157,** 95–134.

Egger, J., 1978: Dynamics of blocking highs. *J. Atmos. Sci.,* **35,** 1788–1801.

Gradshteyn, I. S., and I. M. Ryzhik, 1965: *Table of Integrals, Series and Products.* Academic Press.

Hoskins, B. J., M. E. McIntyre, and A. W. Robertson, 1985: On the use and significance of isentropic potential vorticity maps. *Quart. J. Roy. Meteor. Soc.,* **111,** 877–946.

Machenhauer, B., 1979: The spectral method. *Numerical Methods Used in Atmospheric Models,* Vol. II, WMO/GARP Publ. Ser. 17, 121–275.

McIntyre, M. E., and T. N. Palmer, 1983: Breaking planetary waves in the stratosphere. *Nature,* **305,** 593–600.

Nakamura, M., and R. A. Plumb, 1994: The effects of flow asymmetry on the direction of Rossby wave breaking. *J. Atmos. Sci.,* **51,** 2031–2045.

Pedlosky, J., 1981: Resonant topographic waves in barotropic and baroclinic flows. *J. Atmos. Sci.,* **38,** 2626–2641.

Polvani, L. M., and R. A. Plumb, 1992: Rossby wave breaking, microbreaking, filamentation and secondary vortex formation: The dynamics of a perturbed vortex. *J. Atmos. Sci.,* **49,** 462–476.

——, and D. G. Dritschel, 1993: Wave and vortex dynamics on the surface of a sphere. *J. Fluid Mech.,* **225,** 35–64.

Pullin, D. I., 1992: Contour dynamics methods. *Ann. Rev. Fluid Mech.,* **24,** 89–115.

Queney, P., 1948: The problem of air flow over mountains: A summary of theoretical studies. *Bull. Amer. Meteor. Soc.,* **29,** 16–29.

Saffman, P. G., and R. Szeto, 1980: Equilibrium shapes of a pair of equal uniform vortices. *Phys. Fluids,* **23,** 2339–2342.

Saltzman, B., 1968: Surface boundary effects on the general circulation and macroclimate: A review of the theory of the quasi-stationary perturbations in the atmosphere. *Causes of Climate Change, Meteor. Monogr.,* No. 30, Amer. Meteor. Soc., 4–19.

Verkley, W. T. M., 1994: Tropopause dynamics and planetary waves. *J. Atmos. Sci.,* **51,** 509–529.

Waugh, D. W., 1993: Contour surgery simulations of a forced polar vortex. *J. Atmos. Sci.,* **50,** 714–730.

——, L. M. Polvani, and R. A. Plumb, 1994: Nonlinear, barotropic response to a localized topographic forcing: Formation of a "tropical surf zone" and its effect on interhemispheric propagation. *J. Atmos. Sci.,* **51,** 1401–1416.

Zabusky, N. J., M. H. Hughes, and K. V. Roberts, 1979: Contour dynamics of the Euler equations in two-dimensions. *J. Comput. Phys.,* **30,** 96–106.